

# Green's function retrieval using Marchenko iteration without up/down decomposition: Can the Marchenko algorithm retrieve refracted waves?

Mert S. R. Kiraz<sup>†</sup>, Roel Snieder<sup>†</sup> & Kees Wapenaar<sup>\*</sup>

<sup>†</sup>*Center for Wave Phenomena, Colorado School of Mines, Golden CO 80401, USA*

*email kiraz@mines.edu*

<sup>\*</sup>*Department of Geoscience and Engineering, Delft University of Technology, P.O. Box 5048, Delft, GA 2600, The Netherlands*

## ABSTRACT

Marchenko algorithms retrieve the Green's function for arbitrary subsurface locations, and the retrieved Green's function includes the primary and multiple reflected waves. The Marchenko algorithms require the estimate of the direct arrivals and the reflected waves; however, most previous Marchenko algorithms also require the up/down components of the Marchenko equation for the Green's function retrieval. We use the Marmousi model to retrieve the Green's function without using the up/down components of the Marchenko equation for both two-sided and one-sided illumination cases and show that the retrieved Green's function matches the numerically modeled Green's function fairly well. We also show that the refracted waves can be successfully produced independently from the acquisition geometry, i.e., single-sided or two-sided illumination. However, the retrieval of refracted waves that arrive before the first primary waves is inconsistent with the requirement that the Green's function vanishes before the direct wave. We show that these waves are caused by the injection of the direct wave into sufficiently detailed background velocity and density models instead of the Marchenko algorithm and the operations on the recorded wave fields.

## 1 INTRODUCTION

The Marchenko equation was first introduced by the inverse scattering community to make the connection between the scattered data and the scattering potential, as well as medium reconstruction (Marchenko, 1955; Gel'fand and Levitan, 1955; Agranovich and Marchenko, 1963; Newton, 1980a; Burridge, 1980; Chadan and Sabatier, 1989; Gladwell, 1993; Colton and Kress, 1998). Rose (2001, 2002) utilizes the Marchenko equation for focusing and shows that the solution of the Marchenko equation creates an incident wave field which at  $t = 0$  becomes a delta function at a prescribed focusing location. Broggin and Snieder (2012) make the single-sided autofocusing concept applicable to the seismic exploration studies and show that one can focus the wave field inside the unknown medium using the surface-recorded waves. They also make the connection between the Marchenko equation and seismic interferometry (Weaver and Lobkis, 2001; Derode et al., 2003; Wapenaar et al., 2005; Curtis et al., 2006; Snieder and Larose, 2013) and show that the Green's function can be retrieved without illumination from both sides and without a physical receiver at the virtual source location. Following this, Wapenaar et al. (2013) retrieve the three-dimensional Green's function and provide a two-dimensional example of the Green's function retrieval. Wapenaar et al. (2013) introduce up/down decomposition of the Marchenko equation which constraints the limitations of the Marchenko equation. The up/down decomposition assumes that the wave field at the focal point propagates only in the up-down direction; therefore, the algorithm does not work well at large offsets in layered media where refracted waves and near-surface inhomogeneity zones exist.

Thorbecke et al. (2017) and Lomas and Curtis (2019) discuss how to numerically implement the Marchenko algorithm in detail. van der Neut et al. (2015) also provide an introduction to Marchenko methods. Marchenko methods have been widely used for various applications. Internal multiple reflections can be eliminated using the Marchenko technique (Meles et al., 2015, 2016; Thorbecke et al., 2021). The elastic wave applications of the Marchenko method have also been discussed by da Costa Filho et al. (2014, 2015); Wapenaar (2014). The Marchenko method has also been used for subsurface imaging and artefact-free subsurface

images have been obtained while the conventional RTM results were contaminated due to the spurious events (Behura et al., 2014; Wapenaar et al., 2014a,c; Ravasi et al., 2016; Jia et al., 2018). Wapenaar et al. (2014a) give a thorough description of the Marchenko redatuming and imaging. Additionally, various field data applications of the Marchenko method have been performed including but not limited to the North Sea field dataset (Ravasi et al., 2016), Gulf of Mexico dataset (Jia et al., 2018), Frio carbon sequestration dataset (Kiraz and Nowack, 2018), the Vøring Basin dataset (Wapenaar et al., 2018).

Recently, there have been several studies to address the limitation of the Marchenko method due to the up/down separation of the Marchenko equation. Kiraz et al. (2020) show wave field focusing for an arbitrary point inside an unknown highly scattering inhomogeneous medium using the data acquired on a closed boundary. They show that the Green's function for an arbitrary location in the medium can be retrieved and the retrieved Green's function contains all the scattering effects of the medium, including primary and multiple events. They also show that the Marchenko focusing without up/down decomposition provides better focusing than the direct wave injection focusing. Diekmann and Vasconcelos (2021) and Wapenaar et al. (2021) present alternative approaches to Green's function retrieval without up/down decomposition for single-sided acquisition, each with their own pros and cons.

We present and discuss a new approach to retrieve the full Green's function at an arbitrary depth location in a complicated medium with a series of normal faults, tilted blocks, horizontally layered horizons, variable velocity, and variable density profiles. We extend the algorithm of Rose (2001, 2002) to two dimensions where we have access to either two-sided or one-sided illumination and we show that we can circumvent the up/down component separation of the Marchenko equation to retrieve the full Green's function. We present our numerical examples using the Marmousi model for the two-sided and one-sided illuminations and using two different subsets of the Marmousi model for the one-sided illumination where velocity and density are varying for the Green's function retrieval. We propose an iterative algorithm and we first model the direct wave using the smooth version of the velocity and density models. We then time reverse the direct wave and send it back into the medium from the receiver array. We define a window function between the direct wave and its time-reversed counterpart and apply it to the recorded wave field. The modeled direct wave and the windowed recorded data are then combined and used for the next iteration. The proposed iterative algorithm enables the retrieval of the Green's function at an arbitrary depth location at the Marmousi model. We compare the numerically modeled Green's function to those obtained from the proposed iterative algorithm and present 2D numerical examples. We also show that we can produce the refracted waves caused by the complexity of the Marmousi velocity model but they result from the injection of the direct wave into the smooth background model, they do not result from the Marchenko iteration. By presenting 2D numerical experiments, we show that the retrieved refracted waves have nothing to do with the iterative Marchenko algorithm both in one-sided and two-sided illumination cases; they only depend on the background velocity and density models.

## 2 THEORY

We define the Green's function,  $G(\mathbf{x}, \mathbf{x}_s, t)$ , as the solution to the acoustic wave equation  $LG = \delta(\mathbf{x} - \mathbf{x}_s)\delta(t)$ , with the differential operator  $L = \rho\nabla \cdot (\rho^{-1}\nabla) - c^{-2}\partial^2/\partial t^2$ . Here,  $\mathbf{x}_s$  is the source location and the Green's function is the response to a source at  $\mathbf{x}_s$  recorded at the receiver location  $\mathbf{x}$ . We use the following convention for the Fourier transform:  $f(t) = \frac{1}{2\pi} \int F(\omega) \exp(-i\omega t) d\omega$ , where  $i$  is the imaginary unit. In the frequency domain  $G(\mathbf{x}, \mathbf{x}_s, \omega)$  satisfies  $LG = \delta(\mathbf{x} - \mathbf{x}_s)$ , with the differential operator  $L = \rho\nabla \cdot (\rho^{-1}\nabla) + \omega^2/c^2$ .

We derive the Marchenko iteration without up/down decomposition using a circular acquisition geometry first, and we later extend our method to an acquisition geometry over horizontal surfaces. We define the ingoing wave field,  $U^{in}(\hat{\mathbf{n}}', t)$ , and outgoing wave field,  $U^{out}(\hat{\mathbf{n}}, t)$ , where  $\hat{\mathbf{n}}'$  and  $\hat{\mathbf{n}}$  denote the locations on a circle with radius  $R$  as it is illustrated in Figure 1; the ingoing and outgoing wave fields are related via the scattering response  $A(\hat{\mathbf{n}}, \hat{\mathbf{n}}', t)$  of the inhomogeneous medium. Following Rose (2001, 2002); Broggin and Snieder (2012); Wapenaar et al. (2013, 2014b), we design a wave field that at  $t = 0$  collapses a delta function at the focus location. We start with relating the ingoing wave  $U_k^{in}$  to the outgoing wave  $U_k^{out}$  at iteration  $k$  as

$$U_k^{out}(\hat{\mathbf{n}}, t) = \oint \int A(\hat{\mathbf{n}}, \hat{\mathbf{n}}', t - \tau) U_k^{in}(\hat{\mathbf{n}}', \tau) d\tau dn' . \quad (1)$$

The ingoing and outgoing waves and the scattering operator are defined on a circle with radius  $R$ , but for brevity, we omit the parameter dependence on  $R$  in Eq. (1).

The iterative scheme starts with injecting a delta function into the medium and the ingoing wave field for the first iteration gives

$$U_0^{in}(\hat{\mathbf{n}}', \tau) = \delta(\tau + t_d(\hat{\mathbf{n}}')) , \quad (2)$$

where  $t_d(\hat{\mathbf{n}}')$  is the arrival time of the direct waves that propagates from the focusing point to the point  $\hat{\mathbf{n}}'$  on the circle.

Following Broggin and Snieder (2012), the purpose of the iterative scheme is to reconstruct a wave field that after interacting

with the heterogeneities in the medium collapses onto a delta function at the focusing point at  $t = 0$ . We create a symmetric field in time for  $-t_d(\hat{\mathbf{n}}') < t < t_d(\hat{\mathbf{n}}')$ . We later show that the symmetry in time leads to focusing at  $\mathbf{x}_s$ . To achieve the symmetry for the iterative scheme, we define the ingoing wave field as

$$U_k^{in}(\hat{\mathbf{n}}', \tau) = U_0^{in}(\hat{\mathbf{n}}', \tau) - \Theta(\hat{\mathbf{n}}', \tau) U_{k-1}^{out}(\hat{\mathbf{n}}, -\tau), \quad (3)$$

where  $\Theta(\hat{\mathbf{n}}', \tau)$  is a window function and defined as  $\Theta(\hat{\mathbf{n}}', \tau) = 1$  when  $-t_d(\hat{\mathbf{n}}') < \tau < t_d(\hat{\mathbf{n}}')$ , and otherwise  $\Theta(\hat{\mathbf{n}}', \tau) = 0$ .

When the iterative scheme converges (hence when  $U_k^{out} = U_{k-1}^{out}$ ), the iteration number can be dropped. Inserting Eq. (3) into Eq. (1) then gives

$$U^{out}(\hat{\mathbf{n}}, t) = \oint \int A(\hat{\mathbf{n}}, \hat{\mathbf{n}}', t - \tau) U_0^{in}(\hat{\mathbf{n}}', \tau) d\tau dn' - \oint \int_{-t_d^\epsilon}^{t_d^\epsilon} A(\hat{\mathbf{n}}, \hat{\mathbf{n}}', t - \tau) U^{out}(\hat{\mathbf{n}}', -\tau) d\tau dn', \quad (4)$$

with  $t_d^\epsilon = t_d - \epsilon$  where we introduce  $\epsilon$  as a small positive constant to exclude the direct wave at  $t_d$ . If we define  $K = -U^{out}$ , and substitute this into Eq. (4) using Eq. (2), we obtain

$$K(\hat{\mathbf{n}}, t) + \oint A(\hat{\mathbf{n}}, \hat{\mathbf{n}}', t + t_d(\hat{\mathbf{n}}')) dn' + \oint \int_{-t_d^\epsilon}^{t_d^\epsilon} A(\hat{\mathbf{n}}, \hat{\mathbf{n}}', t - \tau) K(\hat{\mathbf{n}}', -\tau) d\tau dn' = 0. \quad (5)$$

Burridge (1980) shows that the Marchenko equation, Gel'fand-Levitan equation, and the Gopinath-Sondhi equations of inverse scattering can be written in symbolic notation as  $K + R + \int_W RK = 0$  where  $\int_W$  shows the time interval,  $R$  is the recorded data, and  $K$  is the function we will solve for. Eq. (5) has the same structure as the equations derived by Burridge (1980) and, therefore, gives a 2D Marchenko equation without using up/down decomposition. Eq. (5) also has a similar relation with the equations derived by Newton (1980b, 1981, 1982) using the scattering data in multi-dimensional media.

While for the derivations above we assume a recording array on a closed surface, and constant velocity and variable density, we show that the same iterative algorithm can, in practice, be applied to the two-sided illumination using the Marmousi velocity and density models assuming a smooth version of the velocity and density models are available. We use an acquisition geometry over horizontal surfaces by infinitely extending the sides of the domain, and replace the closed surface integral by an integral over two horizontal boundaries. We can, therefore, rewrite Eq. (1) for the two-sided illumination as

$$U_k^{out}(\hat{\mathbf{n}}, t) = \int \int A(\hat{\mathbf{n}}, \hat{\mathbf{n}}', t - \tau) U_k^{in}(\hat{\mathbf{n}}', \tau) d\tau d^2\mathbf{x}, \quad (6)$$

where the integration is over two horizontal boundaries. By following the same steps as above, we can rewrite Eq. (5) for the two-sided illumination as

$$K(\hat{\mathbf{n}}, t) + \int \int A(\hat{\mathbf{n}}, \hat{\mathbf{n}}', t + t_d(\hat{\mathbf{n}}')) d^2\mathbf{x} + \int \int_{-t_d^\epsilon}^{t_d^\epsilon} A(\hat{\mathbf{n}}, \hat{\mathbf{n}}', t - \tau) K(\hat{\mathbf{n}}', -\tau) d\tau d^2\mathbf{x} = 0. \quad (7)$$

Eq. (7) is the same as Eq. (5) except for the integration boundaries which are now reduced to two horizontal boundaries in Eq. (7) from a closed boundary in Eq. (5). Therefore, we can use 2D Marchenko equation without up/down decomposition where we have access to the illumination from two sides.

### 3 NUMERICAL EXAMPLE AND GREEN'S FUNCTION RETRIEVAL

#### 3.1 Green's Function Retrieval for Two-sided Illumination

We start the numerical experiments with the two-sided illumination using the Marmousi velocity model. Figure 2a shows the Marmousi velocity model and the source and receiver geometry of our numerical experiment. Figure 2b shows the smooth version of the Marmousi velocity model. The virtual source location is given by  $x_s = 5$  km and  $z_s = 2$  km in depth. Figure 2c shows the variable density model used for the numerical example and Figure 2d shows the smooth version of the density model. The black asterisk in Figure 2 denotes the virtual source location and the green lines located at the upper and lower boundaries of the models represent the receiver locations. Throughout this study, we use finite-difference modeling with absorbing boundaries where surface-related multiples are excluded in the modeling. The source wavelet is a Ricker with a central frequency of 30 Hz.

For this numerical simulation, we use the two-sided data and only show the wave field recorded at the upper receiver array in Figure 2, and we start the iterative scheme by modeling the direct wave given in Figure 3a using the smooth version of the velocity and the density models given in Figures 2b and 2d, respectively, for the virtual source location denoted with the black asterisk. We use the modeled direct wave in Figure 3a which, after time-reversal, is ingoing when injected into the medium from the receiver

arrays, and use the iterative algorithm to define the outgoing wave field. Figure 3b shows the superposition of the ingoing wave field and the outgoing wave field as  $U^{total}(\mathbf{x}, t) = U^{in}(\mathbf{x}, t) + U^{out}(\mathbf{x}, t)$  for the first iteration. Figure 3c shows  $U^{total}(\mathbf{x}, t)$  for the fourth iteration. The main difference between Figures 3b and 3c is that the wave field in Figure 3c is symmetric in time for times  $-t_d < t < t_d$  (approximately between the tips of the direct arrivals at -1s and 1s), whereas the wave field in Figure 3b is not symmetric in time for  $-t_d < t < t_d$  because it is the output of the first iteration. If we take the difference between the total wave field in Figure 3c and its time-reversed version, i.e.,  $U_{dif} = U_{total}(\mathbf{x}, t) - U_{total}(\mathbf{x}, -t)$ , all events in the interval  $-t_d < t < t_d$  nearly vanish as shown in Figure 3d. Figure 3c shows that the wave field is symmetric in time for  $-t_d < t < t_d$ , hence in Figure 3d they vanish in this interval. Although some energy remains in Figure 3d for  $-t_d < t < t_d$ , this is due to numerical inaccuracies in our solution of the Marchenko equation.

The difference wave field  $U_{dif}$  enables us to create the response to a virtual source located in the subsurface at the focal point without using the up/down decomposition of the Marchenko equation. Figure 3e shows  $U_{dif}$  for the fourth iteration for positive times only and Figure 3f shows the numerically modeled Green's function for the virtual source location. The retrieved Green's function in Figure 3e is similar to the numerically modeled Green's function in Figure 3f for  $t > t_d$ ; however, the retrieved direct waves do not include the refracted waves shown between the receiver numbers 500 and 700. This is due to the smooth version of the velocity and density models used for the iterative scheme that is too smooth to produce refracted waves. The retrieval of refracted waves that arrive before the first primary waves is inconsistent with the requirement that the Green's function vanishes before the direct wave in the smooth reference model. Thus, the Marchenko iteration fails to retrieve the refracted waves. We also compare the individual traces of the retrieved and modeled Green's functions. Figures 4a and 4b show the normalized trace comparison of the estimated and true Green's functions for the receiver number 400 and 500, respectively, for times  $0.8 \text{ s} \leq t \leq 2 \text{ s}$  to emphasize the similarities between the retrieved and modeled Green's function. In Figure 4, the red trace denotes the directly modeled Green's function and the blue trace denotes the retrieved Green's function. Figure 5 shows the Green's function retrieved iteratively without up/down separation (blue lines), superimposed on the directly-modeled Green's function (red lines) for the receiver numbers from 150 to 650. For clarity, the traces have been multiplied by  $\exp(2t)$  to emphasize the scattered waves. As a result of our iterative solution, we retrieve the direct wave and multiply-scattered wave information, and directly modeled and retrieved Green's functions match both in time and amplitude; however, both the right and left edges of the wave field, the tapered zone degrades the match between the retrieved and calculated Green's functions.

The Marchenko iteration without up/down decomposition retrieves the Green's function for an arbitrary subsurface location where we have an access to the illumination from upper and lower boundaries. The retrieved Green's function matches fairly well the numerically modeled Green's function; however, the retrieved Green's function does not include the refracted waves because of the smoothness of the background models used for the direct wave modeling. The two-sided illumination also enables us to use both reflected and transmitted data. The retrieved Green's function, therefore, matches the numerically modeled Green's function. In the following section, we present the one-sided illumination where we only have an access to the reflected data and investigate the comparison between the retrieved and the modeled Green's functions.

### 3.2 Green's Function Retrieval for One-sided Illumination

We present three numerical simulations of the Marchenko without up/down separation using a single-sided receiver array located at the surface. The first example consists of a relatively flat-layered subset of the Marmousi velocity model. Figure 6a shows a subset of the Marmousi velocity model and the source and receiver geometry of our numerical experiment. Figure 6b shows the smooth version of the velocity model. The virtual source location is given by  $x_s = 1 \text{ km}$  and  $z_s = 1.5 \text{ km}$  in depth. Figure 6c shows the variable density model used for the numerical example and Figure 6d shows the smooth version of the density model. The black asterisk in Figure 6 denotes the virtual source location and the green line located at the surface of the models represents the receiver locations.

As we follow the iterative scheme described in section 2, Figure 7a shows the superposition of the ingoing wave field and the outgoing wave field  $U^{total}$  for the first iteration. Figure 7b shows  $U^{total}(\mathbf{x}, t)$  for the sixth iteration. Figure 7b is symmetric in time for the times  $-t_d < t < t_d$ , defined using the arrival time of the direct arrival, for  $-t_d < t < t_d$  (approximately between -1s and 1s). Figure 7c shows  $U_{dif} = U_{total}(\mathbf{x}, t) - U_{total}(\mathbf{x}, -t)$  for the first iteration and Figure 7d shows  $U_{dif} = U_{total}(\mathbf{x}, t) - U_{total}(\mathbf{x}, -t)$  for the sixth iteration. The wave field  $U_{dif}$  in Figure 7c for  $-t_d < t < t_d$  does not vanish whereas the wave field  $U_{dif}$  in Figure 7d for  $-t_d < t < t_d$  cancels out. This cancellation is because of the symmetric wave field for  $-t_d < t < t_d$  in Figure 7b created by the iterative Marchenko algorithm without up/down decomposition. Figure 7e shows  $U_{dif}$  for the sixth iteration for positive times only and Figure 7f shows the numerically modeled Green's function for the virtual source location. The retrieved Green's function in Figure 7e matches the numerically modeled Green's function in Figure 7f for  $t > t_d$ . Figures 8a and 8b show the normalized trace comparison of the estimated and true Green's functions for the receiver numbers 100

and 200, respectively, for times  $0.7 \text{ s} \leq t \leq 2 \text{ s}$ . Figures 8c and 8d show the zoomed-in versions of Figures 8a and 8b for times  $1.4 \text{ s} \leq t \leq 2 \text{ s}$ , respectively. The red trace in Figure 8 denotes the directly modeled Green's function and the blue trace denotes the retrieved Green's function. As a result of our iterative solution, we retrieve the direct and multiply-scattered waves, and for both time windows in Figure 8, directly modeled and retrieved Green's functions match very accurately both in time and amplitude. Figure 9 shows the Green's function retrieved iteratively without up/down separation (blue lines), superimposed on the directly-modeled Green's function (red lines). For clarity, the traces have been multiplied by  $\exp(2t)$  to emphasize the scattered waves. As a result of our iterative solution, we retrieve the direct wave and multiply-scattered wave information, and directly modeled and retrieved Green's functions match both in time and amplitude; however, at both right and left edges of the wave field, the tapered zone reduces the match between the retrieved and calculated direct waves.

The second example consists of a geologically more complicated subset of the Marmousi velocity model than the first example. Figure 10a shows a subset of the Marmousi velocity model and the source and receiver geometry of our numerical experiment. Figure 10b shows the smooth version of the velocity model. The virtual source location is given by  $x_s = 1 \text{ km}$  and  $z_s = 2.3 \text{ km}$  in depth. Figure 10c shows the variable density model used for the numerical example and Figure 10d shows the smooth version of the density model. The black asterisk in Figure 10 denotes the virtual source location and the green line located at the surface of the models represents the receiver locations.

We use the Marchenko iteration without up/down decomposition to retrieve the Green's function and Figure 11a shows  $U_{dif}$  for the sixth iteration for positive times only. Figure 11b shows the numerically modeled Green's function for the virtual source location. The retrieved Green's function in Figure 11a matches the numerically modeled Green's function in Figure 11b for  $t > t_d$ . We further take a close look at individual traces to see the similarities between the retrieved and the modeled Green's functions. Figures 12a and 12b show the normalized trace comparison of the estimated and true Green's functions for the receiver numbers 100 and 200, respectively, for times  $0.85 \text{ s} \leq t \leq 2 \text{ s}$ . Figures 12c and 12d show the zoomed-in versions of Figures 12a and 12b for times  $1.4 \text{ s} \leq t \leq 2 \text{ s}$ , respectively. The red trace in Figure 12 denotes the directly modeled Green's function and the blue trace denotes the retrieved Green's function. As a result of our iterative solution, despite this complicated subsurface model and the single-sided acquisition surface, we retrieve the direct and multiply-scattered waves, and for both time windows in Figure 12, directly modeled and retrieved Green's functions match very accurately both in time and amplitude. The trace-view comparison of the retrieved and the modeled Green's functions provide a better comparison than the grayscale images. Figure 13 shows the Green's function retrieved iteratively without up/down separation (blue lines), superimposed on the directly-modeled Green's function (red lines). For clarity, the traces have been multiplied by  $\exp(2t)$  to emphasize the scattered waves. As a result of the iterative Marchenko without up/down separation using the single-sided acquisition, we retrieve the direct wave and multiply-scattered wave information, and directly modeled and retrieved Green's functions match both in time and amplitude; however, at both right and left edges of the wave field, the used tapering reduces the match between the retrieved and calculated direct waves.

As the last numerical example of the one-sided illumination experiment, we use the Marmousi model to retrieve the Green's function for the virtual source location  $\mathbf{x}_s$  where we have an access to the surface acquisition array only. Figure 14a shows the Marmousi velocity model and the source and receiver geometry of our numerical experiment where we have a one-sided receiver array located at the upper boundary of the medium. Figure 14b shows the smooth version of the Marmousi velocity model. The virtual source location is given by  $x_s = 5 \text{ km}$  and  $z_s = 2 \text{ km}$  in depth. Figure 14c shows the variable density model used for the numerical example and Figure 14d shows the smooth version of the density model. The black asterisk in Figure 14 denotes the virtual source location and the green line located at the upper boundary of the models represents the receiver locations.

We retrieve the Green's function for the virtual source location using the Marchenko iteration without wave field decomposition. Figure 15a shows  $U_{dif}$  for the sixth iteration for positive times only and Figure 15b shows the numerically modeled Green's function for the virtual source location. Different from the other one-sided illumination examples, this time the retrieved Green's function in Figure 15a does not match the numerically modeled Green's function in Figure 15b for  $t > t_d$ . Figure 16a shows the normalized trace comparison of the estimated and true Green's functions for the receiver numbers 400 for times  $0.8 \text{ s} \leq t \leq 2 \text{ s}$ . Figure 16b shows the zoomed-in versions of the traces in Figure 16a for times  $1.4 \text{ s} \leq t \leq 2 \text{ s}$ . The red trace in Figure 16 denotes the directly modeled Green's function and the blue trace denotes the retrieved Green's function. The traces in Figure 16 show that the numerically modeled Green's function and the retrieved Green's function do not match except for the direct wave. The mismatch between the retrieved and modeled Green's functions in this example is due to the complexity of the medium and the limited receiver aperture at the upper boundary of the Marmousi model. The limited acquisition array prevents the iterative scheme from retrieving the Green's function for an arbitrary subsurface location in this complicated subsurface model. The two-sided illumination used for the Marmousi model, however, retrieves the Green's function fairly well (see Figures 4 and 5) because of the receiver arrays located at the upper and lower boundaries of the Marmousi model.

We also compare the retrieved Green's function for the one- and two-sided illuminations in the Marmousi model. The green

line in Figure 17a shows the retrieved Green’s function using one-sided illumination and the black line in Figure 17a shows the retrieved Green’s function using two-sided illumination for the positive times from 0.8 to 2 s. Figure 17b shows the same traces for the limited times from 1.4 to 2 s. Figure 17 shows that the major difference between the two traces is the amplitude mismatch for the waves arriving after the direct wave (approximately after 0.9 s). Although the traces match better for the times  $t > 1.7$  s (Figure 17b) than they match for the times  $0.8 \text{ s} \leq t \leq 1.7 \text{ s}$  (Figure 17a), the overall match is poor. This shows that in order to retrieve the Green’s function using the Marchenko iteration without up/down decomposition for the Marmousi model, one will need the two-sided illumination from the upper and lower boundaries.

We apply the Marchenko iteration without up/down decomposition where we have an access to an array located on the surface to two different subsets of the Marmousi model and the Marmousi model. The first two examples show that our methodology successfully retrieves the Green’s function for an arbitrary subsurface location with the single-sided acquisition geometry although we originally derive the iterative algorithm for the acquisition geometry with a closed receiver array. However, the last example shows that the Marchenko iteration without up/down decomposition fails to retrieve the Green’s function using one-sided illumination in the structurally complicated parts of the Marmousi model when the focusing point is deep. Although the one-sided application of the Marchenko iteration without up/down decomposition requires a rigorous mathematical derivation to prove the following argument, we can claim that the Marchenko iteration without up/down decomposition can be used to retrieve the Green’s function for an arbitrary subsurface location using single-sided receiver array where we are interested in moderately complicated subsurface models (e.g., Figures 6 and 10), but is not able to perform well for very complicated subsurface models (e.g., Figure 14). Wapenaar et al. (2021) give a detailed derivation of the Green’s function representations without relying on the wave field decomposition below a single horizontal acquisition boundary. The two-sided illumination provides an access to reflected and transmitted data and the retrieved Green’s function matches the numerically modeled Green’s function better than the one-sided illumination results. The numerical examples given in this section show that the proposed Marchenko iteration without up/down decomposition can also be used for the one-sided illumination experiments although we derive the theory for the aperture with a closed boundary. Figures 7e, 7f, 8, and 9 show that the proposed algorithm retrieves the Green’s function very well; however, Figures 11-13; 15 and 16 show that as the subsurface model gets more complicated, the retrieved and modeled Green’s functions become less similar. We also point out that the virtual source location used throughout this experiment is deliberately chosen at a deep subsurface location. Using a shallower focal point provides a better match between the retrieved and the numerically modeled Green’s functions since the overburden above the focal point contains fewer complicated features. For the sake of testing our algorithm and finding its limits, we keep the focal point at a location close to the lower boundary of the medium for the numerical experiments. While these observations are a topic of future research, we conclude that the Marchenko iteration without up/down decomposition can be used for the one-sided illumination studies, and as the subsurface model gets more complicated, the retrieved Green’s function will become less similar to the modeled Green’s function.

#### 4 RETRIEVAL OF REFRACTED WAVES

For the two-sided illumination, Figure 3e shows that for positive times, the wave field  $U_{total}(\mathbf{x}, t) - U_{total}(\mathbf{x}, -t)$  vanishes to some extent at the receivers for  $t < t_d$ . If we consider this wave field at  $t = 0$ , the direct waves radiated at  $t = 0$  from  $\mathbf{x}_s$  arrive at a receiver location  $\mathbf{x}_R$  at  $t_d$ . If we suppose that waves would radiate at  $t = 0$  from a point  $\mathbf{x} \neq \mathbf{x}_s$ , for some receivers, those waves would arrive at a time  $t < t_d$ ; however, as shown in Figure 3e, no waves arrive at time  $t < t_d$ . This means that waves do not radiate from any point  $\mathbf{x} \neq \mathbf{x}_s$  at  $t = 0$ , and the retrieved wave field, therefore, is, up to a multiplicative constant, the Green’s function. While these assumptions are valid for the closed recording array and two-sided illumination cases, we show that this algorithm retrieves the Green’s function for an arbitrary subsurface location with the one-sided illumination. The numerical examples in section 3 show that the Green’s function retrieval using one-sided Marchenko without up/down decomposition and the retrieved and modeled Green’s functions match well for the first two examples. The examples also show that the Green’s function for a virtual source location in the subsurface can be obtained without using the decomposition of the Marchenko equation. However, the last numerical example in section 3 shows that there is a limitation to the subsurface model complexity in order for the iterative algorithm to retrieve the Green’s function.

The retrieved Green’s function shown in Figure 3e matches the numerically modeled Green’s function in Figure 3f except for the refracted waves, and Figures 4 and 5 show that the Marchenko algorithm without up/down decomposition retrieves the primary and multiple events for the variable velocity and density Marmousi model. However, because we inject the wave field from a limited aperture (the green lines in Figure 2) back into the medium in the iterative process, we use a taper on both right and left edges of the wave field to suppress truncation artefacts. Therefore, the right and left sides of the retrieved Green’s function are reduced by the taper, leading to a poor match of the retrieved and the modeled Green’s function around the edges of the receiver aperture.

The major difference between the retrieved and the modeled Green's function occurs around the direct arrivals for the two-sided illumination. The modeled Green's function in Figure 3f shows that due to the virtual source location and complexity of the medium, refracted waves are present in the recorded Green's function; however, the retrieved Green's function in Figure 3e does not include the refracted waves around the direct arrivals. The lack of the refracted waves in the retrieved Green's function is due to the smoothness of the velocity and density models used to model the direct arrivals. For comparison, Figures 18a and 18b show a less smooth version of the velocity and density models, respectively, than the one we use in the iterative process for the same source and receiver locations. Figure 18c shows the numerically modeled direct wave using the smooth velocity and density models in Figures 2b and 2d, respectively. Figure 18d shows the numerically modeled direct wave using the smooth velocity and density models in Figures 18a and 18b, respectively. Figure 18d shows the directly modeled refracted waves whereas Figure 18c does not include the modeled refracted waves. The labels R1, R2, and R3 point to the wave field positions where the refracted waves occur. Using these smoothed velocity and density models, Figure 18e shows the retrieved Green's function without up/down decomposition and the labels point to refracted waves that are not present in Figure 3e. The retrieved Green's functions in Figures 3e and 18e, are analogous for times when  $t > t_d$ . This indicates that the proposed Marchenko algorithm without up/down decomposition retrieves the primaries and multiples; however, the retrieved refracted waves do not come from the Marchenko iterations but depend on the spatial variations of the velocity and density models used to model the direct arrivals.

The one-sided illumination does suffice to include the refracted waves using a less smooth version of the velocity and density models. Figure 18f shows an estimate of the Green's function from the direct wave injection only from the upper acquisition boundary (upper green line) in Figure 18a and the labels R1, R2, and R3 denote the recorded refracted waves. The refracted waves are present despite the single-sided acquisition and despite the fact that the direct wave injection does not include any iterations of the Marchenko algorithm. Figures 18c and 18d show that the refracted waves depend only on the initial estimates of the velocity and density models and on the injection of the direct wave. The acquisition boundary, either one-sided or two-sided, and the iterations of the Marchenko algorithm do not affect the recorded refracted waves. Figure 18f also shows that the refracted waves even with the direct wave injection match well with the numerically modeled refracted waves (see Figure 18d). The direct wave injection produces the refracted waves and this shows that the retrieval of these refracted waves is not the result of the Marchenko algorithm. While these observations still require further investigation, we claim that the accurateness of the refracted waves in this experiment depends only on the initial estimate of the velocity and density models, rather than on the iterative processing of recorded waves in the Marchenko algorithm.

## 5 CONCLUSIONS

We present the Green's function retrieval without up/down decomposition using the Marmousi model for both two-sided and one-sided illuminations. For the two-sided illumination the Green's function is reconstructed accurately, but for the one-sided illumination the reconstructed Green's function is fairly accurate for focusing points in simple parts of the model; however, the reconstruction degrades with model complexity and increasing depth of the focusing point. We show that the proposed Marchenko iteration without up/down decomposition can be successfully applied to two-sided and one-sided apertures. For the one-sided aperture, the retrieved Green's function does not match the numerically modeled Green's function for the full Marmousi model whereas the algorithm suffices to retrieve the Green's function for different subsets of the Marmousi model using the one-sided aperture. Understanding the quality of Green's function reconstruction as a function of focusing depth and model complexity is a topic of future investigation. We successfully produce the refracted waves in the retrieved Green's function when detailed velocity and density information are available for the initial estimate of the direct waves. We compare the effects of the background velocity and density models for one-sided and two-sided illumination on producing the refracted waves. Our numerical experiments show that the recorded refracted waves only depend on the initial estimates of the velocity and density models, and are not a result of the Marchenko algorithm. The refracted waves can be produced even at the first iteration when the velocity and density models have detailed information about the subsurface, these refracted waves do not arise because of the iterative Marchenko algorithm.

## 6 ACKNOWLEDGMENTS

This work is supported by the Consortium Project on Seismic Inverse Methods for Complex Structures at the Colorado School of Mines. The reproducible numerical examples in this paper were generated using the Madagascar software package (<http://www.ahay.org>). The research of K. Wapenaar has received funding from the European Research Council (grant no. 742703).

## REFERENCES

- Agranovich, Z., and V. Marchenko, 1963, The inverse problem of scattering theory: Gordon and Breach.
- Behura, J., K. Wapenaar, and R. Snieder, 2014, Autofocus imaging: Image reconstruction based on inverse scattering theory: *GEOPHYSICS*, **79**, A19–A26.
- Broggini, F., and R. Snieder, 2012, Connection of scattering principles: A visual and mathematical tour: *European Journal of Physics*, **33**, no. 3, 593–613.
- Burridge, R., 1980, The Gelfand-Levitan, the Marchenko, and the Gopinath-Sondhi integral equations of inverse scattering theory, regarded in the context of inverse impulse-response problems: *Wave Motion*, **2**, 305–323.
- Chadan, K., and P. C. Sabatier, 1989, *Inverse problems in quantum scattering theory*: Springer.
- Colton, D., and R. Kress, 1998, *Inverse acoustic and electromagnetic scattering theory*: Springer.
- Curtis, A., P. Gerstoft, H. Sato, R. Snieder, and K. Wapenaar, 2006, Seismic interferometry – turning noise into signal: *The Leading Edge*, **25**, 1082–1092.
- da Costa Filho, C. A., M. Ravasi, and A. Curtis, 2015, Elastic p- and s-wave autofocus imaging with primaries and internal multiples: *GEOPHYSICS*, **80**, S187–S202.
- da Costa Filho, C. A., M. Ravasi, A. Curtis, and G. A. Meles, 2014, Elastodynamic Green’s function retrieval through single-sided Marchenko inverse scattering: *Phys. Rev. E*, **90**, no. 6, 063201.
- Derode, A., E. Larose, M. Campillo, and M. Fink, 2003, How to estimate the Green’s function for a heterogeneous medium between two passive sensors? Application to acoustic waves: *Appl. Phys. Lett.*, **83**, 3054–3056.
- Diekmann, L., and I. Vasconcelos, 2021, Focusing and Green’s function retrieval in three-dimensional inverse scattering revisited: A single-sided Marchenko integral for the full wave field: *Phys. Rev. Research*, **3**, no. 1, 013206.
- Gel’fand, I., and B. Levitan, 1955, On the determination of the differential equation from its spectral function: *Amer. Math. Soc. Transl. (2)*, **1**, 253–304.
- Gladwell, G. M. L., 1993, *Inverse problems in scattering*: Kluwer Academic Publishing.
- Jia, X., A. Guitton, and R. Snieder, 2018, A practical implementation of subsalt Marchenko imaging with a gulf of mexico data set: *GEOPHYSICS*, **83**, S409–S419.
- Kiraz, M. S. R., and R. L. Nowack, 2018, Marchenko redatuming and imaging with application to the Frio carbon sequestration experiment: *Geophysical Journal International*, **215**, 1633–1643.
- Kiraz, M. S. R., R. Snieder, and K. Wapenaar, 2020, Marchenko focusing without up/down decomposition: *SEG Technical Program Expanded Abstracts 2020*, 3593–3597.
- Lomas, A., and A. Curtis, 2019, An introduction to Marchenko methods for imaging: *GEOPHYSICS*, **84**, F35–F45.
- Marchenko, V., 1955, The construction of the potential energy from the phases of scattered waves: *Dokl. Akad. Nauk*, **104**, 695–698.
- Meles, G. A., K. Löer, M. Ravasi, A. Curtis, and C. A. da Costa Filho, 2015, Internal multiple prediction and removal using Marchenko autofocusing and seismic interferometry: *GEOPHYSICS*, **80**, A7–A11.
- Meles, G. A., K. Wapenaar, and A. Curtis, 2016, Reconstructing the primary reflections in seismic data by Marchenko redatuming and convolutional interferometry: *GEOPHYSICS*, **81**, Q15–Q26.
- Newton, R. G., 1980a, Inverse scattering. I. one dimension: *Journal of Mathematical Physics*, **21**, 493–505.
- , 1980b, Inverse scattering. II. three dimensions: *Journal of Mathematical Physics*, **21**, 1698–1715.
- , 1981, Inverse scattering. III. three dimensions, continued: *Journal of Mathematical Physics*, **22**, 2191–2200.
- , 1982, Inverse scattering. IV. three dimensions: generalized Marchenko construction with bound states, and generalized Gel’fand–Levitan equations: *Journal of Mathematical Physics*, **23**, 594–604.
- Ravasi, M., I. Vasconcelos, A. Kritski, A. Curtis, C. A. d. C. Filho, and G. A. Meles, 2016, Target-oriented Marchenko imaging of a North Sea field: *Geophysical Journal International*, **205**, 99–104.
- Rose, J. H., 2001, “Single-sided” focusing of the time-dependent Schrödinger equation: *Physical Review A*, **65**, no. 1, 012707.
- , 2002, Time reversal, focusing and exact inverse scattering. in: Fink m., kuperman w.a., montagner jp., tourin a. (eds) *imaging of complex media with acoustic and seismic waves. topics in applied physics*, vol 84: Springer, Berlin, Heidelberg.
- Snieder, R., and E. Larose, 2013, Extracting Earth’s elastic wave response from noise measurements: *Ann. Rev. Earth Planet. Sci.*, **41**, 183–206.
- Thorbecke, J., E. Slob, J. Brackenhoff, J. van der Neut, and K. Wapenaar, 2017, Implementation of the Marchenko method: *GEOPHYSICS*, **82**, WB29–WB45.
- Thorbecke, J., L. Zhang, K. Wapenaar, and E. Slob, 2021, Implementation of the Marchenko multiple elimination algorithm: *GEOPHYSICS*, **86**, F9–F23.

- van der Neut, J., K. Wapenaar, J. Thorbecke, E. Slob, and I. Vasconcelos, 2015, An illustration of adaptive Marchenko imaging: *The Leading Edge*, **34**, 818–822.
- Wapenaar, K., 2014, Single-sided Marchenko focusing of compressional and shear waves: *Phys. Rev. E*, **90**, no. 6, 063202.
- Wapenaar, K., J. Brackenhoff, J. Thorbecke, J. van der Neut, E. Slob, and E. Verschuur, 2018, Virtual acoustics in inhomogeneous media with single-sided access: *Scientific Reports*, **8**, 2497.
- Wapenaar, K., F. Brogini, E. Slob, and R. Snieder, 2013, Three-dimensional single-sided Marchenko inverse scattering, data-driven focusing, Green's function retrieval, and their mutual relations: *Phys. Rev. Lett.*, **110**, no. 8, 084301.
- Wapenaar, K., J. Fokkema, and R. Snieder, 2005, Retrieving the Green's function in an open system by cross correlation: A comparison of approaches (L): *The Journal of the Acoustical Society of America*, **118**, no. 5, 2783–2786.
- Wapenaar, K., R. Snieder, S. de Ridder, and E. Slob, 2021, Green's function representations for Marchenko imaging without up/down decomposition: [arXiv:2103.07734](https://arxiv.org/abs/2103.07734).
- Wapenaar, K., J. Thorbecke, J. van der Neut, F. Brogini, E. Slob, and R. Snieder, 2014a, Marchenko imaging: *Geophysics*, **79**, no. 3, WA39–WA57.
- , 2014b, Marchenko imaging: *GEOPHYSICS*, **79**, WA39–WA57.
- Wapenaar, K., J. Thorbecke, J. van der Neut, I. Vasconcelos, and E. Slob, 2014c, Marchenko imaging below an overburden with random scatterers: **2014**, 1–5.
- Weaver, R., and O. Lobkis, 2001, Ultrasonics without a source: Thermal fluctuation correlations at MHz frequencies: *Physical Review Letters*, **87**, no. 13, 134301.

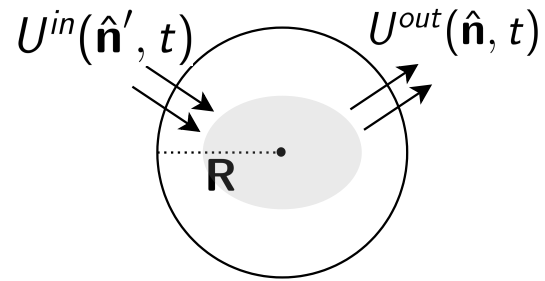


**Figure 1.** Illustration of the ingoing ( $U^{in}(\hat{\mathbf{n}}', t)$ ) and outgoing ( $U^{out}(\hat{\mathbf{n}}, t)$ ) wave fields for ingoing and outgoing locations  $\hat{\mathbf{n}}'$  and  $\hat{\mathbf{n}}$ , on a circle with radius  $R$ , respectively.

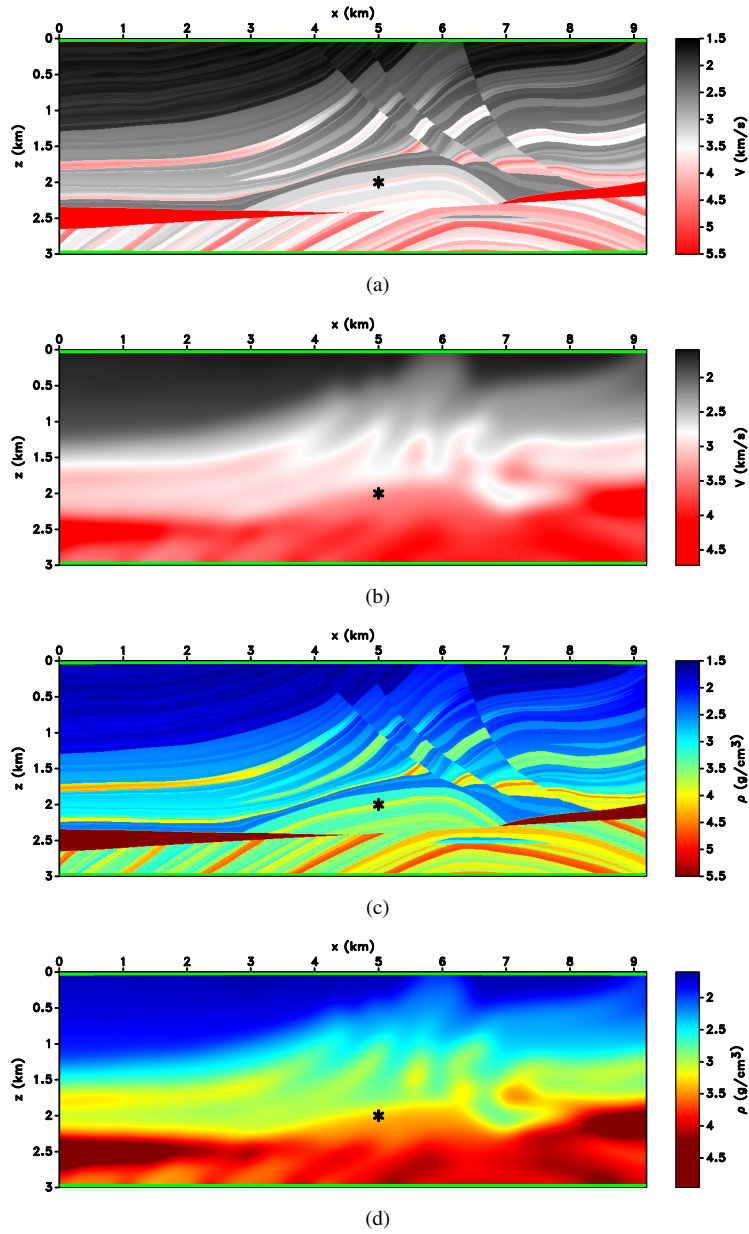


**Figure 2.** (a) The Marmousi velocity model. (b) Smooth version of the Marmousi velocity model. (c) Density model. (d) Smooth version of the density model. The black asterisk shows the virtual source location and the green lines at the top and bottom indicate the source/receiver lines.

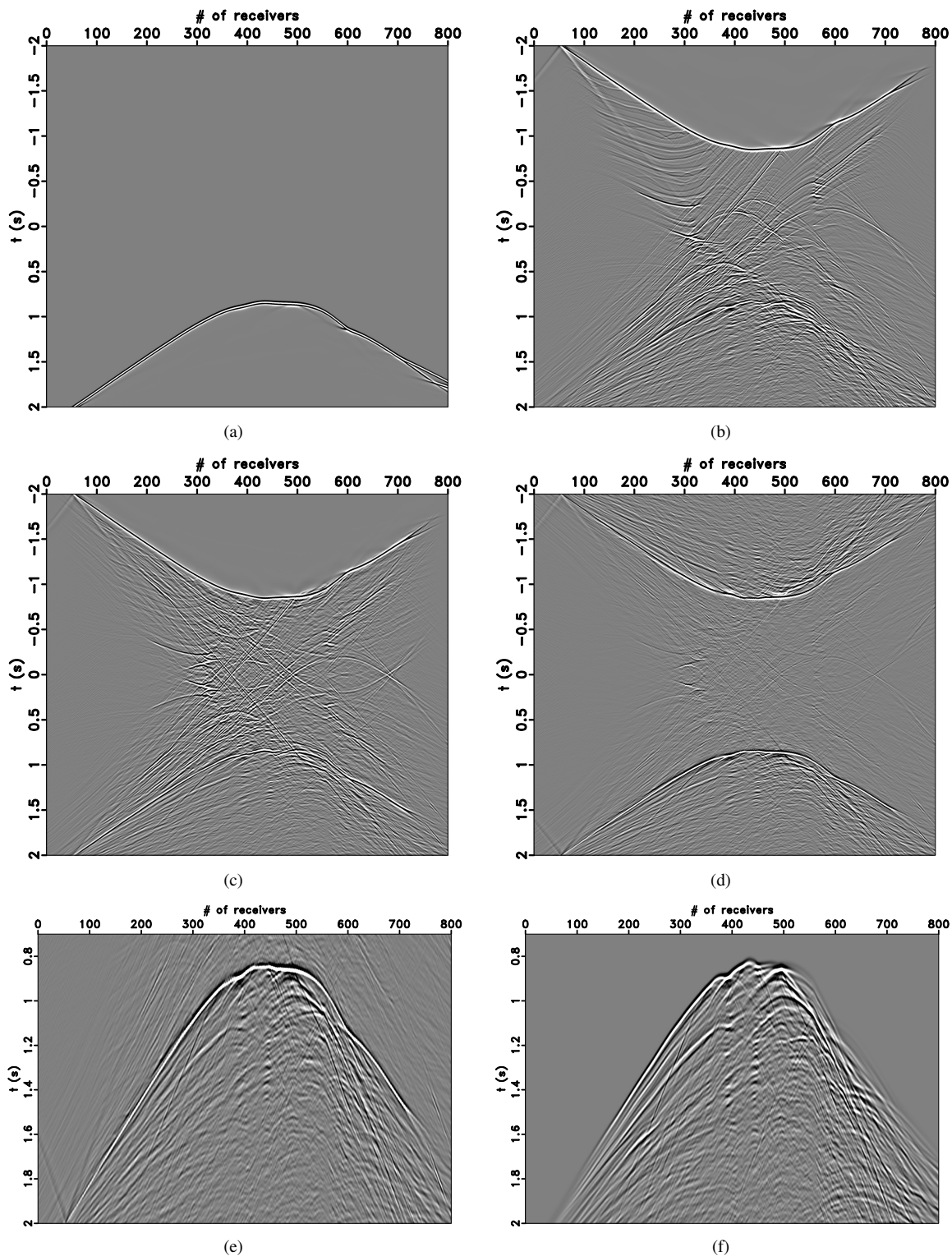


**Figure 3.** (a) The modeled direct wave using the smooth velocity and density models in Figures 2b and 2d, respectively. (b)  $U_{total}(\mathbf{x}, t)$  for the first iteration. (c)  $U_{total}(\mathbf{x}, t)$  for the fourth iteration. (d)  $U_{total}(\mathbf{x}, t) - U_{total}(\mathbf{x}, -t)$  for the fourth iteration. (e) The retrieved Green's function using the iterative algorithm. (f) The numerically modeled Green's function.

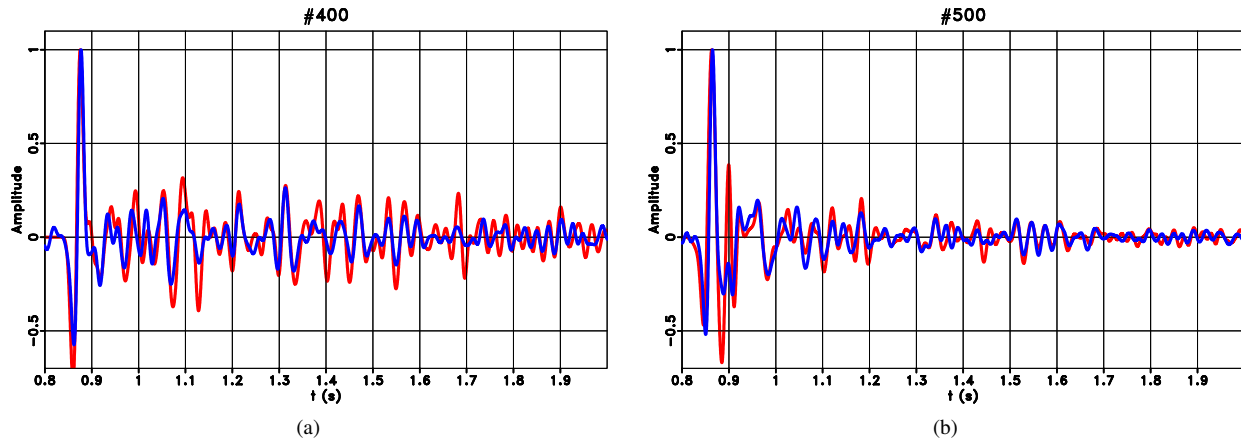


**Figure 4.** (a) The 400th normalized trace of the retrieved Green's function (blue line) and the numerically modeled Green's function (red line). (b) The 500th normalized trace of the retrieved Green's function (blue line) and the numerically modeled Green's function (red line).

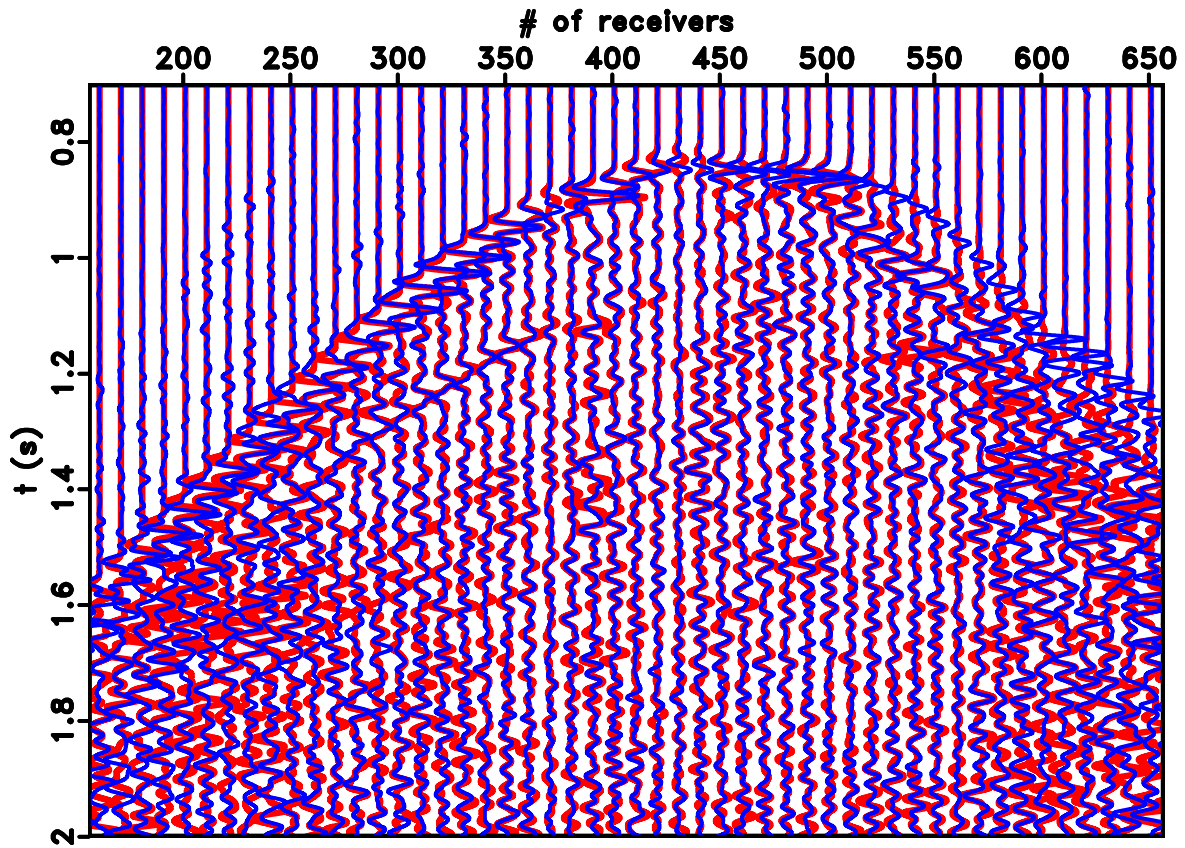


**Figure 5.** The calculated (red line) and the retrieved (blue line) Green's functions. The traces have been multiplied by  $\exp(2t)$  to emphasize the scattered waves.

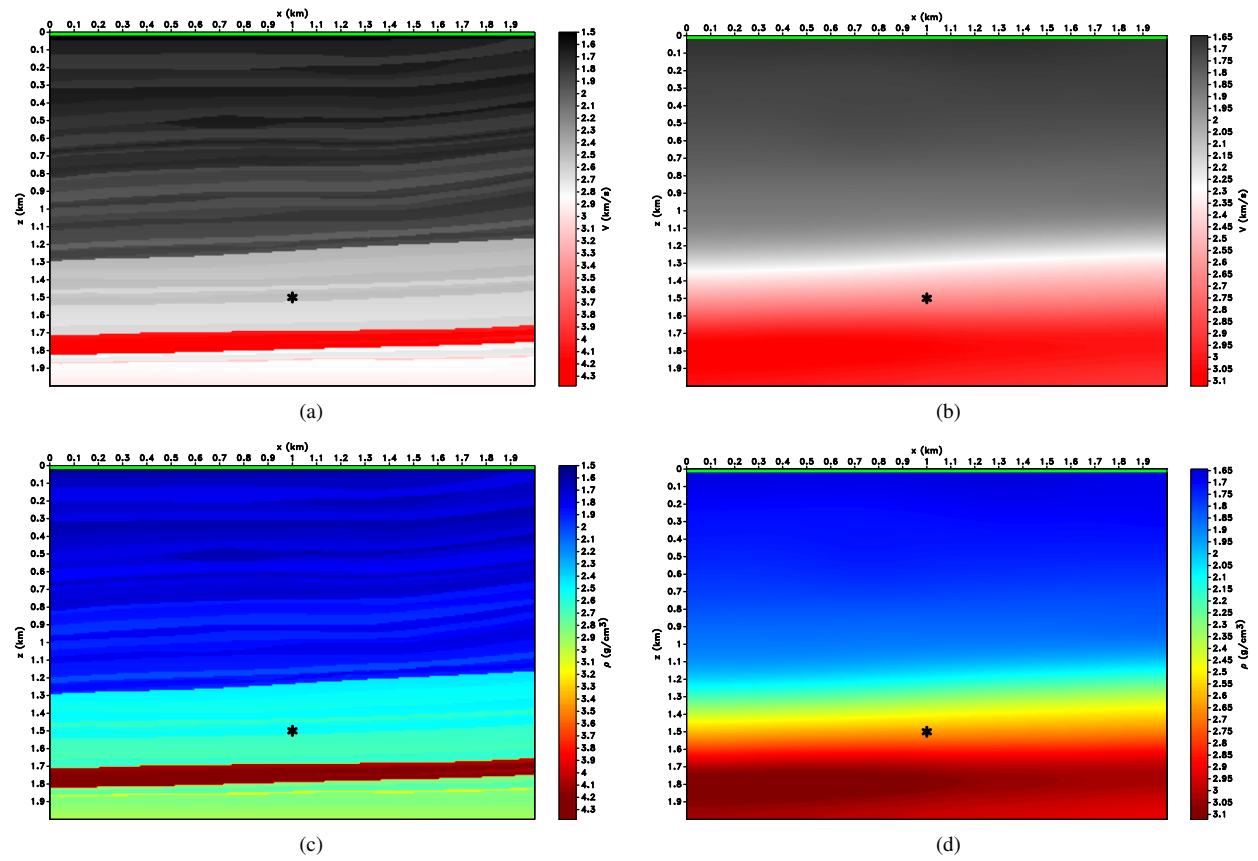


**Figure 6.** (a) A subset of the Marmousi velocity model. (b) Smooth version of the velocity model. (c) Density model. (d) Smooth version of the density model. The black asterisk shows the virtual source location and the green line at the top indicates the source/receiver line.

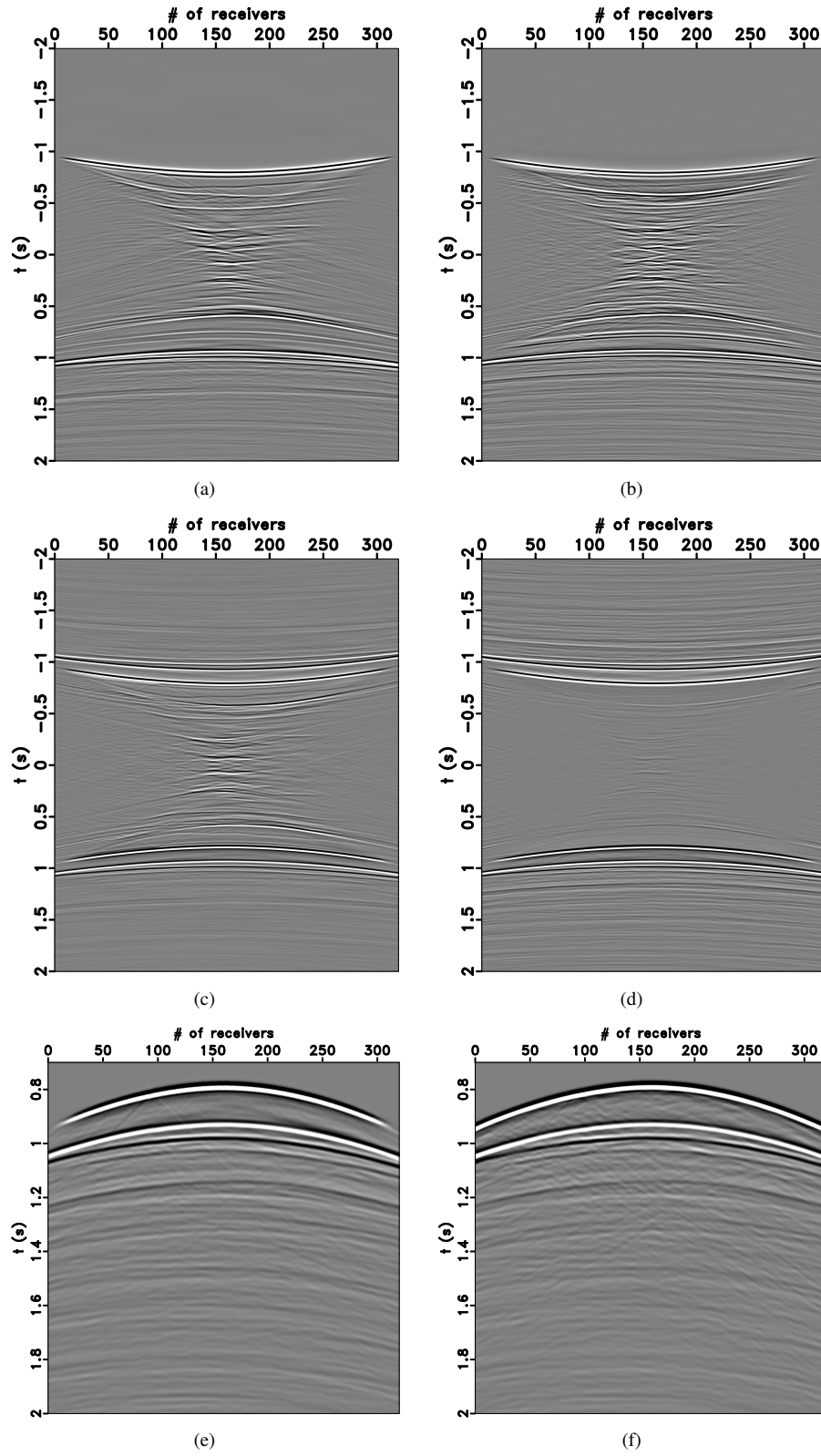


**Figure 7.** (a)  $U_{total}(\mathbf{x}, t)$  for the first iteration. (b)  $U_{total}(\mathbf{x}, t)$  for the sixth iteration. (c)  $U_{total}(\mathbf{x}, t) - U_{total}(\mathbf{x}, -t)$  for the first iteration. (d)  $U_{total}(\mathbf{x}, t) - U_{total}(\mathbf{x}, -t)$  for the sixth iteration. (e) The retrieved Green's function using the iterative algorithm. (f) The numerically modeled Green's function.

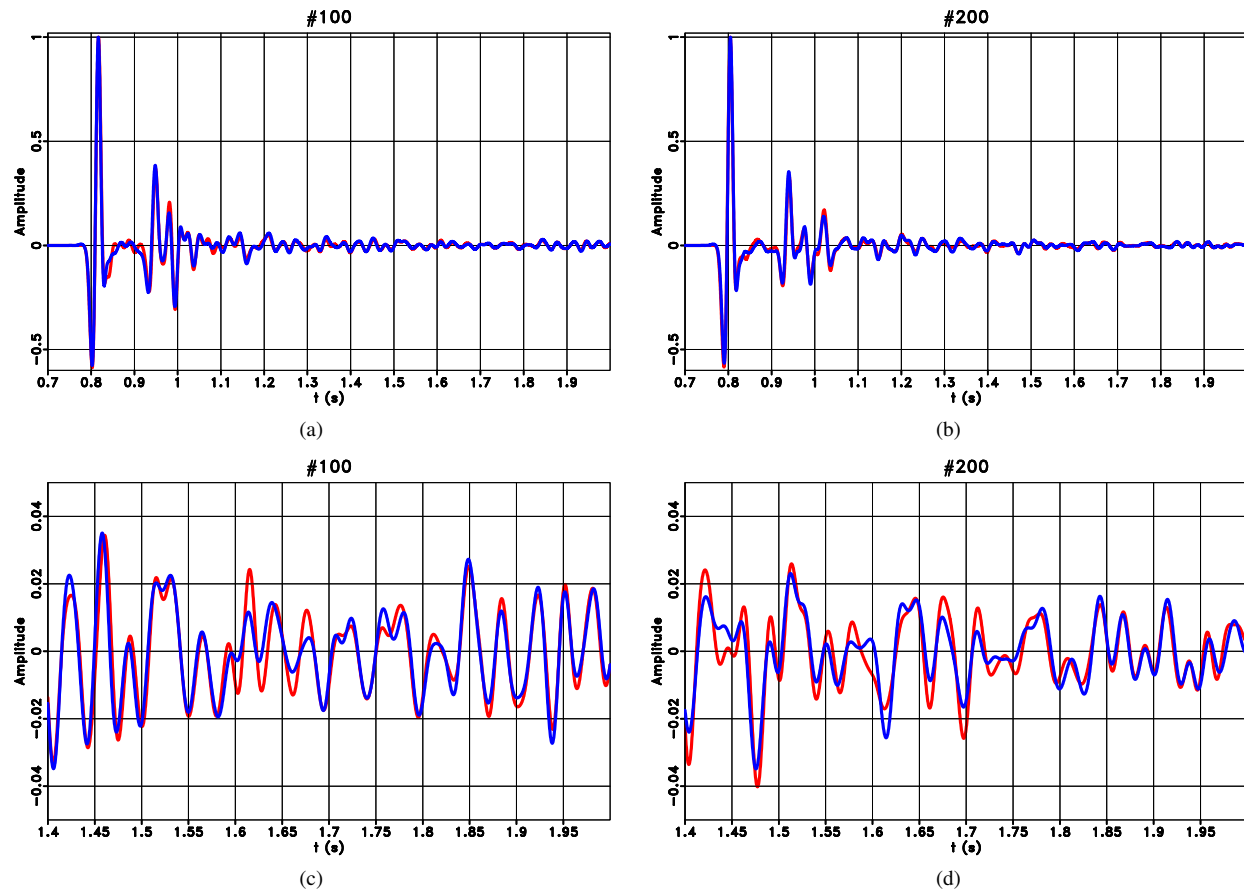


**Figure 8.** (a) The 100th normalized trace of the retrieved Green's function (blue line) and the numerically modeled Green's function (red line). (b) The 200th normalized trace of the retrieved Green's function (blue line) and the numerically modeled Green's function (red line). (c) Limited time interval of the traces in (a) for times from 1.4 to 2 s. (d) Limited time interval of the traces in (b) for times from 1.4 to 2 s.

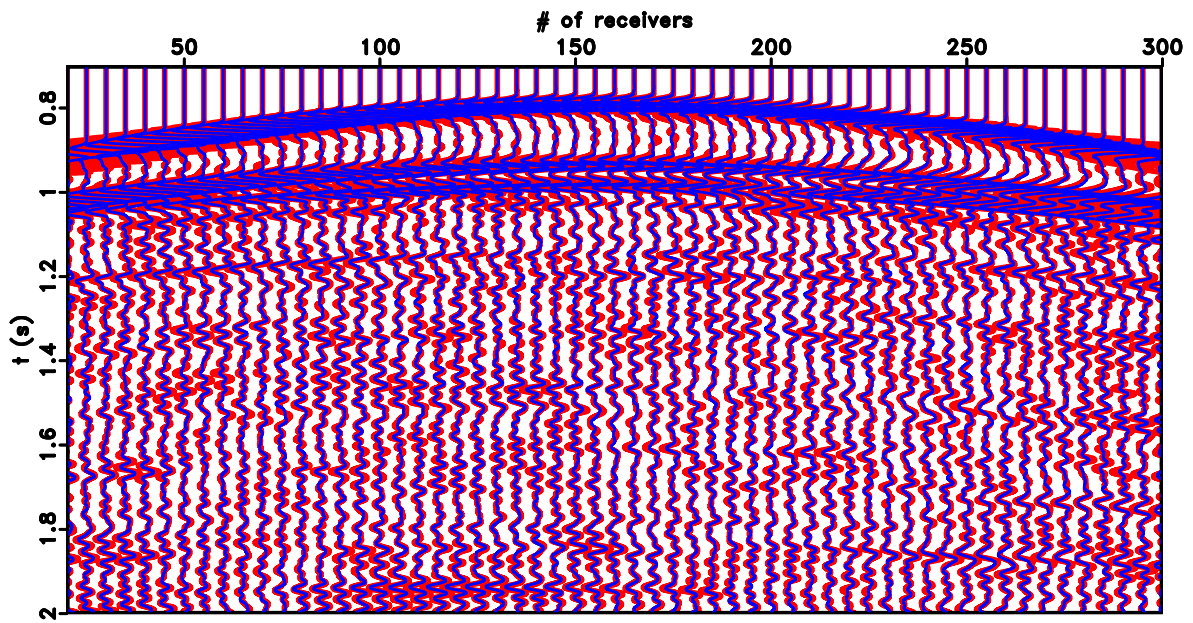


**Figure 9.** The calculated (red line) and the retrieved (blue line) Green's functions. The traces have been multiplied by  $\exp(2t)$  to emphasize the scattered waves.

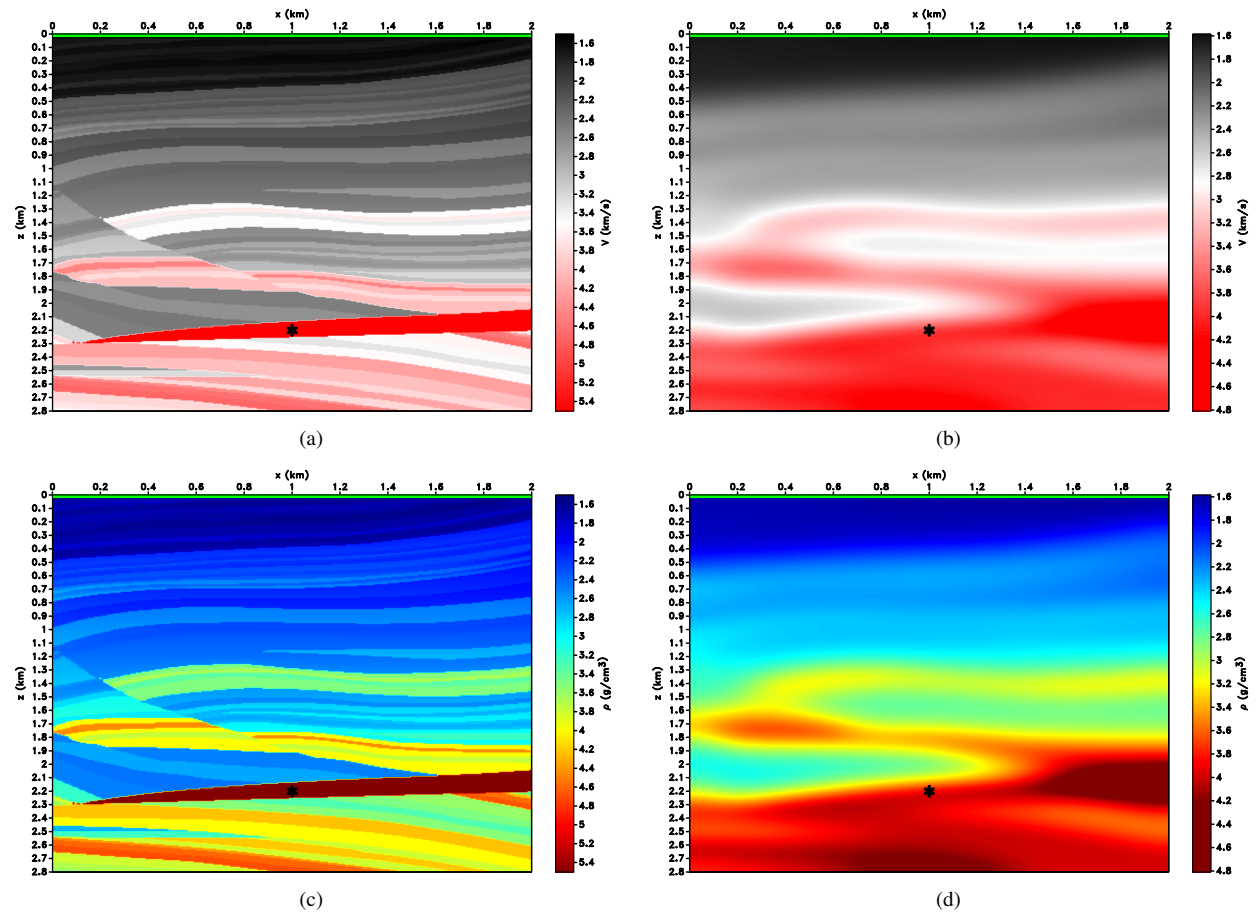
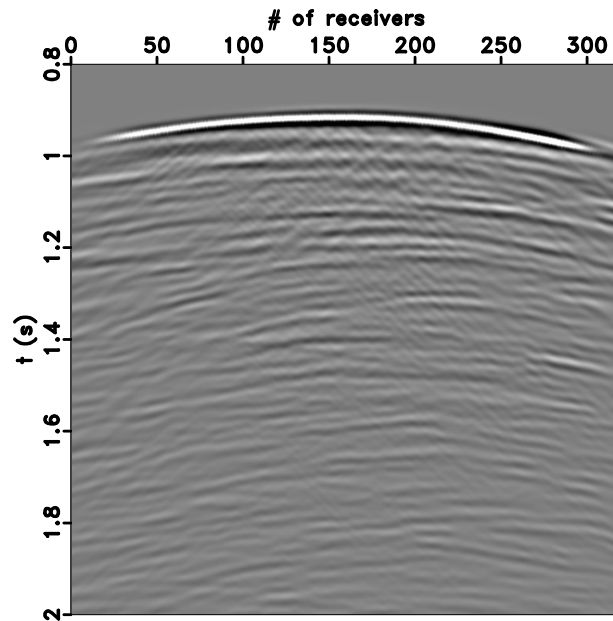
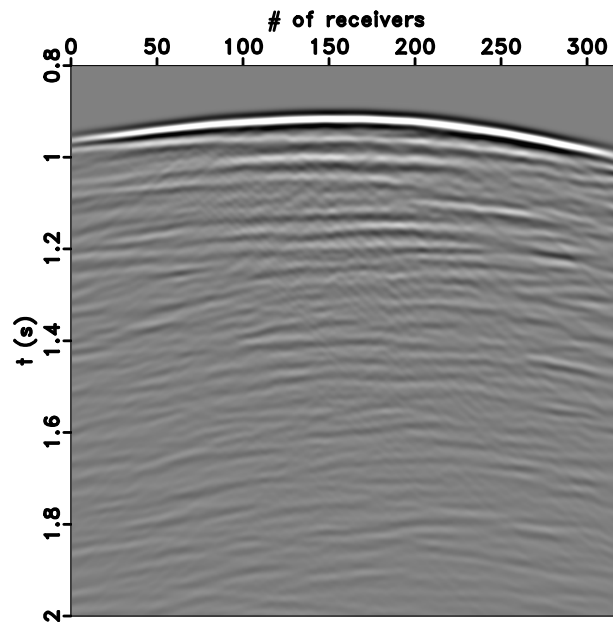


**Figure 10.** (a) A subset of the Marmousi velocity model. (b) Smooth version of the velocity model. (c) Density model. (d) Smooth version of the density model. The black asterisk shows the virtual source location and the green line at the top indicates the source/receiver line.



(a)



(b)

**Figure 11.** (a) The retrieved Green's function using the iterative algorithm. (b) The numerically modeled Green's function.

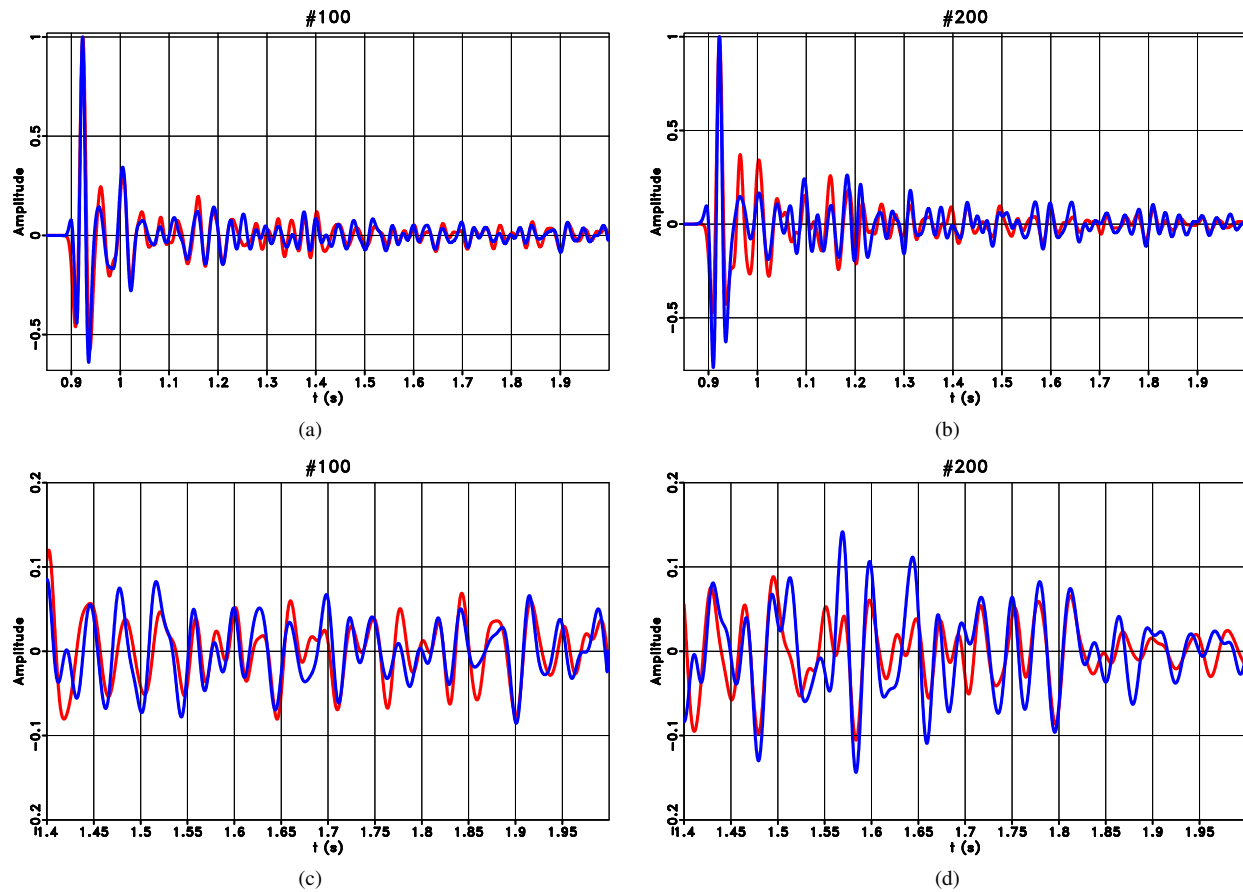


**Figure 12.** (a) The 100th normalized trace of the retrieved Green's function (blue line) and the numerically modeled Green's function (red line). (b) The 200th normalized trace of the retrieved Green's function (blue line) and the numerically modeled Green's function (red line). (c) Limited time interval of the traces in (a) for times from 1.4 to 2 s. (d) Limited time interval of the traces in (b) for times from 1.4 to 2 s.

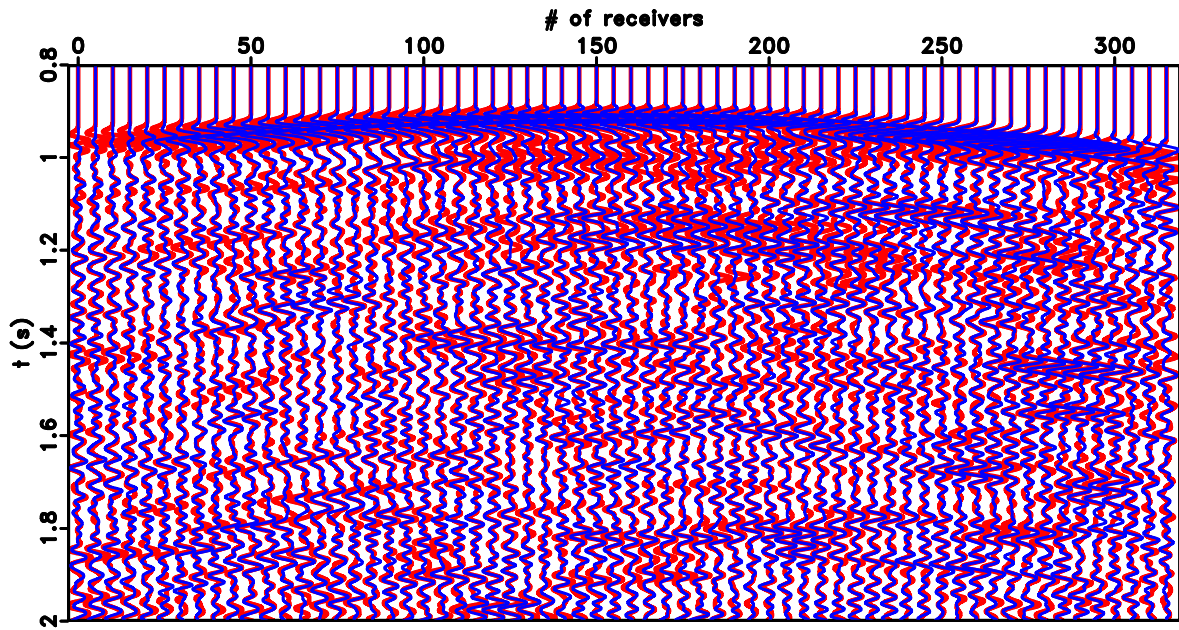


**Figure 13.** The calculated (red line) and the retrieved (blue line) Green's functions. The traces have been multiplied by  $\exp(2t)$  to emphasize the scattered waves.

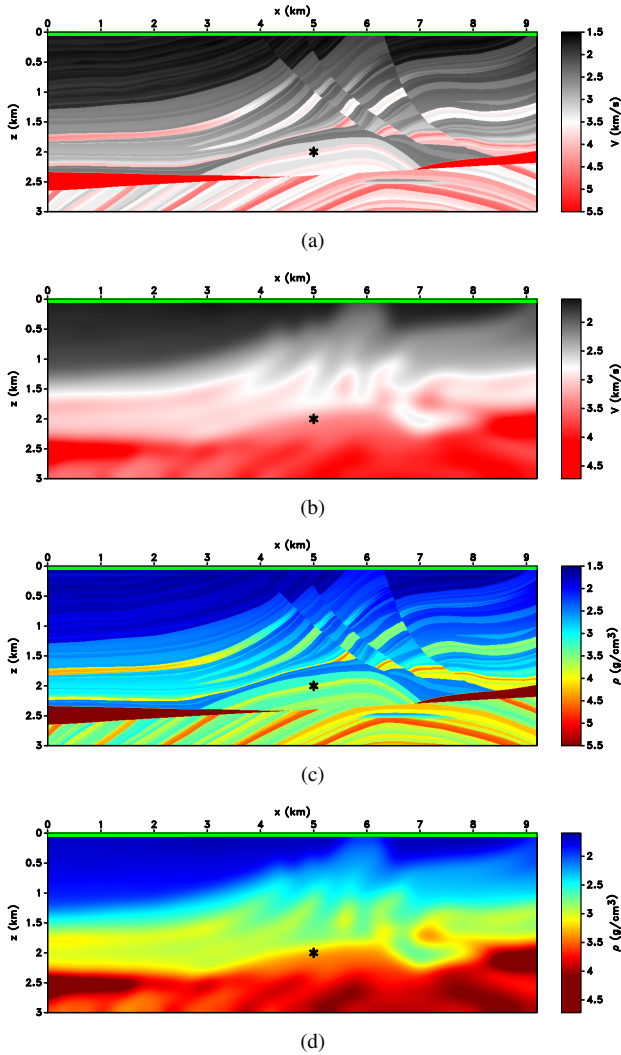
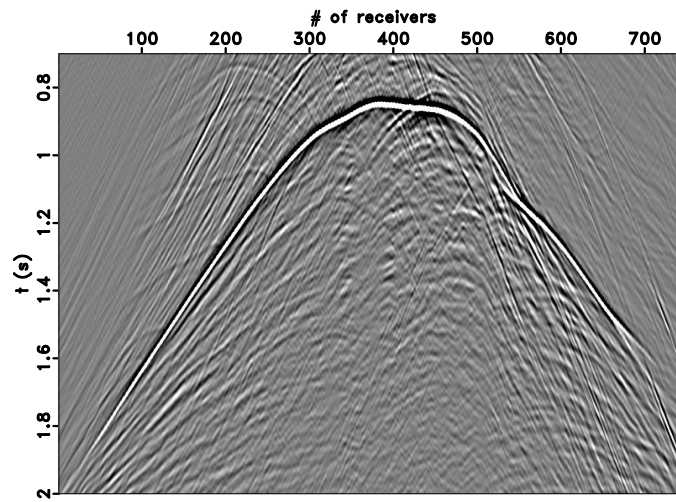
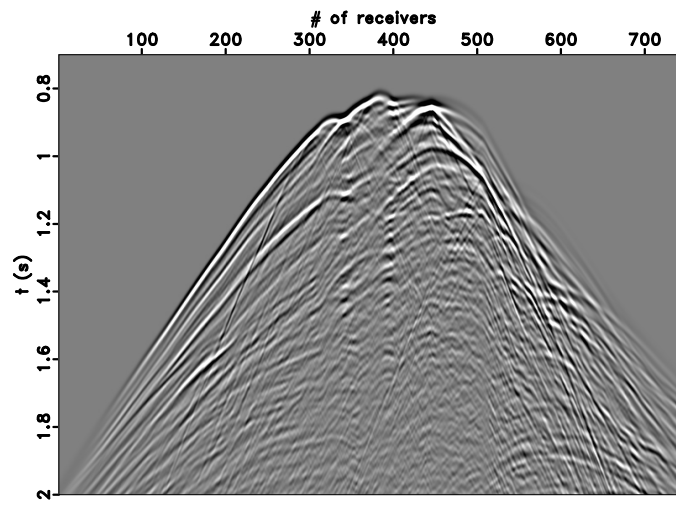


**Figure 14.** (a) The Marmousi velocity model. (b) Smooth version of the Marmousi velocity model. (c) Density model. (d) Smooth version of the density model. The black asterisk shows the virtual source location and the green line at the top indicates the source/receiver line.



(a)



(b)

**Figure 15.** (a) The retrieved Green's function using the iterative algorithm. (b) The numerically modeled Green's function.

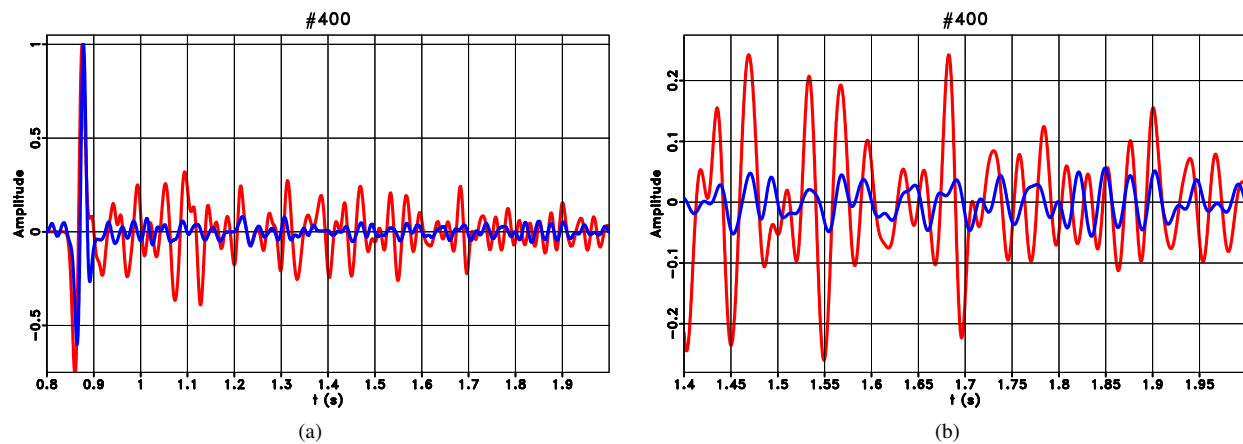


**Figure 16.** (a) The 400th normalized trace of the retrieved Green's function (blue line) and the numerically modeled Green's function (red line). (b) Limited time interval of the traces in (a) for times from 1.4 to 2 s.

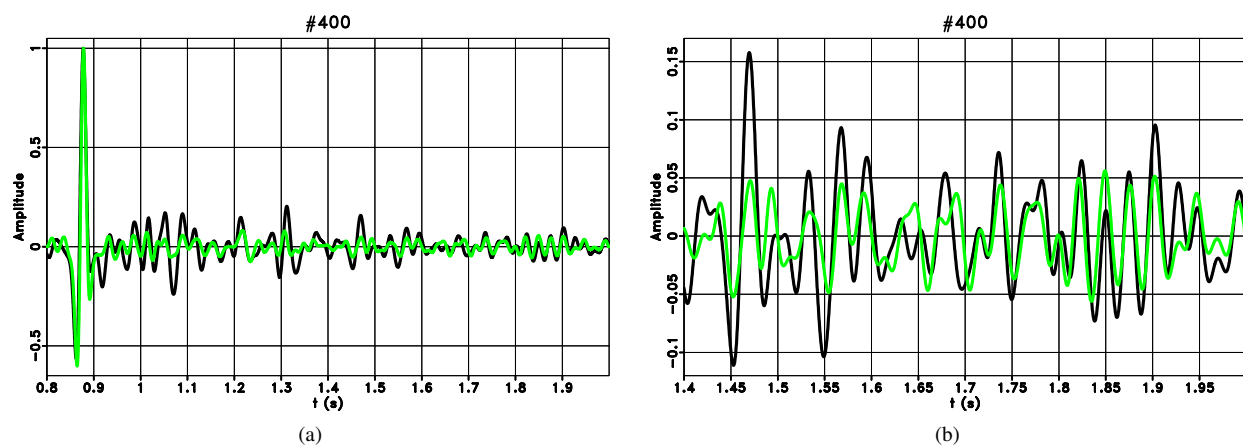


**Figure 17.** (a) The 400th normalized trace of the retrieved Green's function using two-sided recording arrays (black line) and the retrieved Green's function using one-sided recording arrays (green line). (b) Limited time interval of the traces in (a) for times from 1.4 to 2 s.

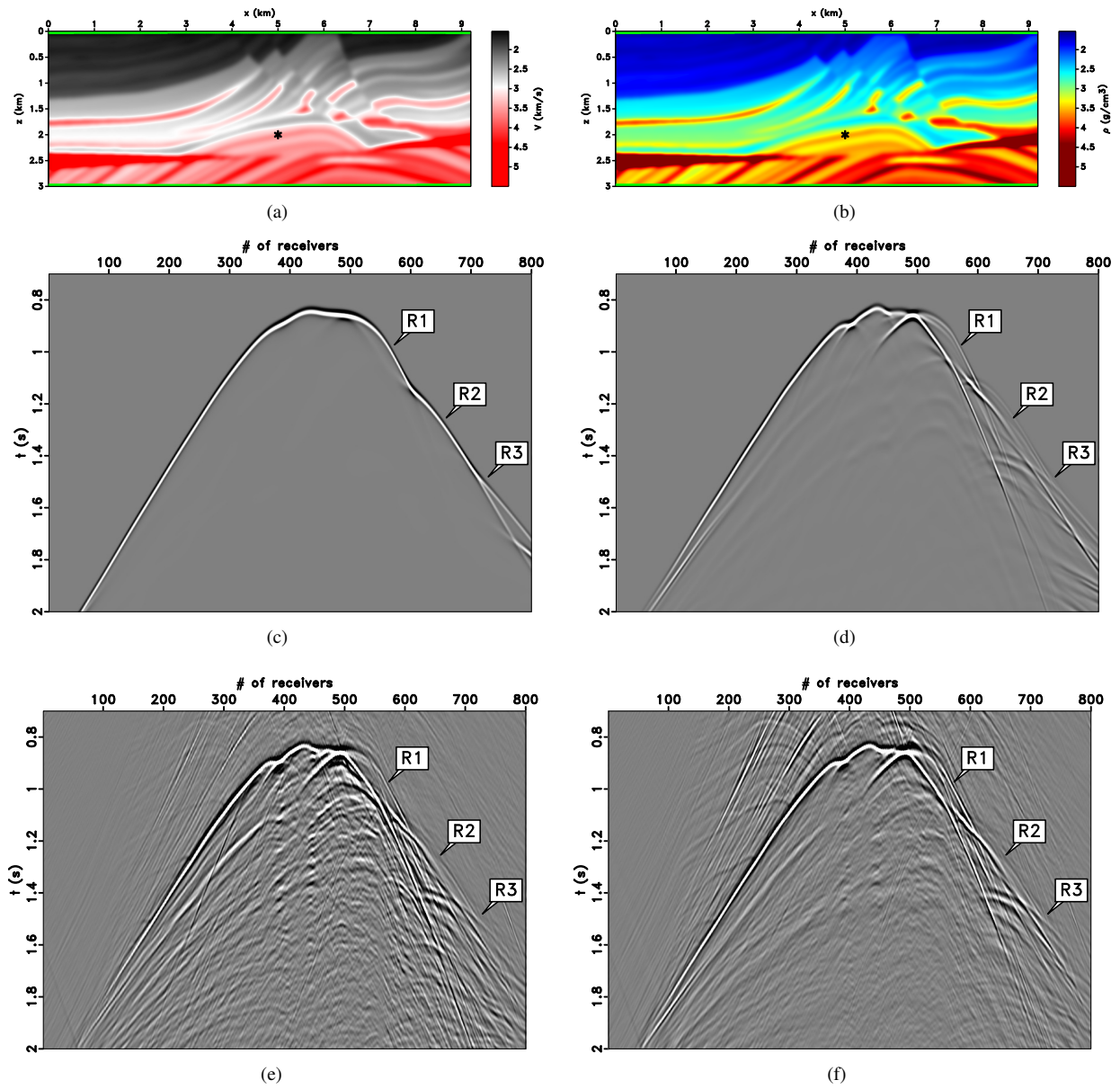


**Figure 18.** (a) Smooth version of the velocity model. (b) Smooth version of the density model. (c) The modeled direct wave using the smooth velocity and density models in Figures 2b and 2d, respectively. (d) The modeled direct wave using the smooth velocity and density models in (a) and (b), respectively. (e) The retrieved Green's function. (f) The retrieved Green's function using only the upper acquisition boundary.